Supplementary information for:

Fano Resonances in the Photoinduced H-Atom Elimination Dynamics in $\pi\sigma^*$ States of Pyrrole

Sergy Yu. Grebenshchikov* and David Picconi

Department of Chemistry, Technische Universität München,

Lichtenbergstr. 4, 85747 Garching, Germany

I. AB INITIO MOLECULAR HAMILTONIAN

A. The Hamiltonian

(1) The molecular Hamiltonian for the ground electronic state and the lowest two excited $^1\pi\sigma^*$ states,

$$\hat{H} = \begin{pmatrix} \hat{T} & 0 & 0 \\ 0 & \hat{T} & 0 \\ 0 & 0 & \hat{T} \end{pmatrix} + \begin{pmatrix} V^X & V^{XA_2} & V^{XB_1} \\ V^{XA_2} & V^{A_2} & V^{A_2B_1} \\ V^{XB_1} & V^{A_2B_1} & V^{B_1} \end{pmatrix} , \tag{1}$$

is set in the basis of three locally diabatic electronic states X, A_2, and B_1. Pyrrole is described using (a) three Jacobi coordinates $\mathbf{R} \equiv (R, \theta, \phi)$ of the dissociating H-atom relative to the center of mass of the pyrrolyl fragment (the so-called 'disappearing modes'; see Fig. S1) and (b) 21 dimensionless normal modes $\mathbf{Q}$ of pyrrolyl, calculated at the equilibrium geometry of the fragment (the so-called 'non-disappearing modes'; examples of them are given in Fig. S2). The normal modes $\mathbf{Q}$ are partitioned into four blocks according to the irreps Γ of the C_{2v} symmetry group, $\mathbf{Q} = \{\mathbf{Q}_{a1}, \mathbf{Q}_{a2}, \mathbf{Q}_{b1}, \mathbf{Q}_{b2}\}$.

(2) The kinetic energy operator in Eq. (1) is set in the body-fixed principal axis frame for the zero total angular momentum of pyrrole (atomic units are used hereafter):

$$\hat{T} = -\frac{1}{2\mu}\frac{\partial^2}{\partial R^2} - \frac{1}{2}\sum_{\Gamma=a_1,a_2,b_1,b_2}\sum_i{}^{\Gamma}\omega_\Gamma(i)\frac{\partial^2}{\partial Q_\Gamma(i)^2} + \frac{\boldsymbol{j}^2}{2\mu R^2} + \frac{1}{2}\left(\frac{j_x^2}{I_x} + \frac{j_y^2}{I_y} + \frac{j_z^2}{I_z}\right) . \tag{2}$$

The first term is the kinetic energy of the relative motion of the H-atom and pyrrolyl; μ is the corresponding reduced mass. The second term refers to pyrrolyl vibrations; the

* Electronic mail: Sergy.Grebenshchikov@ch.tum.de

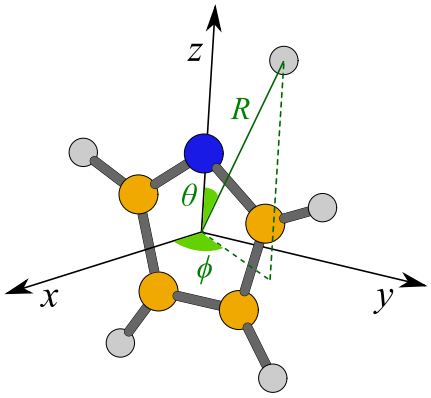

FIG. S1: Body-fixed pyrrolyl axes and Jacobi coordinates (R, θ, ϕ) for the detaching H atom in pyrrole (H - gray; C - orange; N - blue).

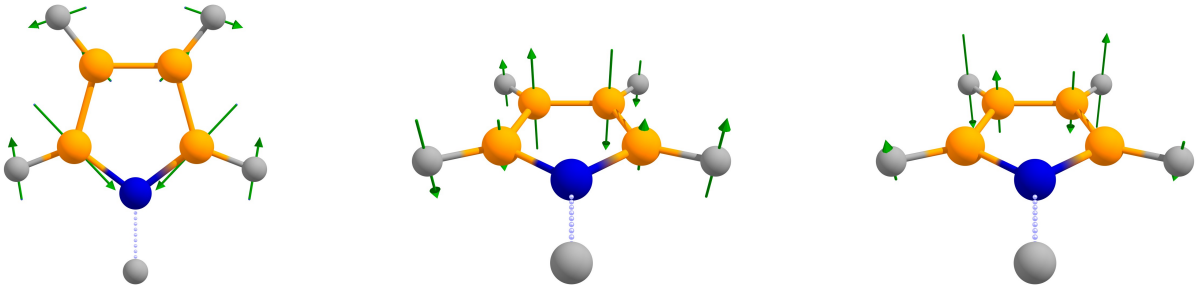

$Q_{a1}(5)$ ($\omega = 1558$ cm^{-1}) $Q_{a2}(1)$ ($\omega = 533$ cm^{-1}) $Q_{a2}(3)$ ($\omega = 932$ cm^{-1})

FIG. S2: Pyrrolyl normal modes used in the quantum mechanical calculations. The a_1 modes are the totally symmetric in-plane distorsions. The out-of-plane a_2 modes are antisymmetric with respect to the reflection planes σ_v, σ_v' and symmetric with respect to rotations about the C_2 axis.

sum $\sum_i^\Gamma$ runs over the vibrational modes i belonging to the irrep Γ. The last two terms describe the orbital motion of the H-atom and the rotational motion of the rigid pyrrolyl ring; $\boldsymbol{j} = (j_x, j_y, j_z)$ is the pyrrolyl angular momentum operator and the inertia constants I_x, I_y and I_z are evaluated at the fragment equilibrium geometry; the C_{2v} symmetric pyrrolyl ring lies in the yz-plane, with z being the C_2 axis (see Fig. S1).

(3) The elements of the diabatic potential energy matrix in Eq. (1) are constructed as sums of two groups of terms,

$$\boldsymbol{V}(\mathbf{R}, \mathbf{Q}) = \boldsymbol{V}_R(\mathbf{R}) + \boldsymbol{V}_Q(\mathbf{Q}|\mathbf{R}) \tag{3}$$

Functions $\boldsymbol{V}_R(\mathbf{R})$ of the three disappearing modes are constructed using spline interpolations of the ab initio points calculated on a dense coordinate grid (R, θ, ϕ). Functions $\boldsymbol{V}_Q(\mathbf{Q}|\mathbf{R})$,

depending on the 21 non-disappearing modes $\mathbf{Q}$, are constructed in the spirit of the vibronic coupling model,[1] with pyrrolyl treated as a semirigid ring using quadratic Hamiltonians, and parameters depending on the interfragment distance R.

(4) The diagonal elements V^α have the form ($\alpha = X, A_2, B_1$):

$$V^\alpha(R,\theta,\phi,\mathbf{Q}) \;=\; V_R^\alpha(R,\theta,\phi) + \sum_i^{a_1} \kappa_i^\alpha(R) Q_{a_1}(i) + \frac{1}{2}\sum_\Gamma \sum_{i,j}^{\Gamma} \gamma_{\Gamma,ij}^\alpha(R) Q_\Gamma(i) Q_\Gamma(j)\,. \quad (4)$$

where $\kappa_i^\alpha(R)$ are the R-dependent gradients (vanishing for all modes but a_1) and $\gamma_{ij}^\alpha(R)$ are the R-dependent normal mode Hessian matrices evaluated at $\mathbf{Q} = \mathbf{0}$; matrices γ^α are four-block diagonal: $\boldsymbol{\gamma}^\alpha = \boldsymbol{\gamma}_{a_1}^\alpha \oplus \boldsymbol{\gamma}_{a_2}^\alpha \oplus \boldsymbol{\gamma}_{b_1}^\alpha \oplus \boldsymbol{\gamma}_{b_2}^\alpha$.

(5) The off-diagonal diabatic couplings $V^{\alpha\beta}$ are

$$V^{\alpha\beta}(R,\theta,\phi,\mathbf{Q}) = V_R^{\alpha\beta}(R,\theta,\phi) + \sum_i^{\Gamma_\alpha\times\Gamma_\beta} \lambda_i^{\alpha\beta}(R) Q_{\Gamma_\alpha\times\Gamma_\beta}(i)\;. \quad (5)$$

The functions $V_R^{\alpha\beta}(R,\theta,\phi)$ are the coupling elements between the regularized quasi-diabatic states constructed on the ab initio coordinate grid using the algorithm of Köppel et al.[2] Although they do not have a simple analytical representation, they follow the lowest allowed orders in the symmetry-adapted spherical harmonics near conical intersections, namely $V_R^{A_1A_2} \sim \sin^2\theta \sin(2\phi)$ and $V_R^{A_1B_1} \sim \sin\theta\cos\phi$. The $\mathbf{Q}$-dependent coupling terms for X/A_2 and X/B_1 are linear in the vibrational modes of a_2 and b_1 symmetry, respectively. The coupling matrix element $V^{A_2B_1}$ between the states A_2/B_1 is not included in the quantum mechanical calculations.

(6) The quasi-diabatic representation of the Hamiltonian of Eq. (1) is local, and a given off-diagonal matrix element is non-zero only in the vicinity of the respective conical intersection. For the second term in Eq. (5), this is achieved by the attenuation of the coupling strength $\lambda_i^{\alpha\beta}$ outside a strip of width Δ around the conical intersection,

$$\lambda_i^{\alpha\beta}(R) = \lambda_{\mathrm{CI},i}^{\alpha\beta} \exp\left(-\left|\frac{R - R_{\mathrm{CI}}^{\alpha\beta}}{\Delta}\right|^n\right)\;, \quad (6)$$

where $R_{\mathrm{CI}}^{\alpha\beta}$ is the position of a conical intersection between $\alpha/\beta = X/A_2$ or X/B_1. The parameters $\lambda_{\mathrm{CI},i}^{\alpha\beta}$, Δ and n are tuned 'by eye' in order to obtain smooth diabatic Hessians for the coupled states. For the first term in Eq. (5), similar attenuation functions are applied to the (R,θ,ϕ)-dependent mixing angles of the regularized adiabatic-to-diabatic transformation.

B. Ab initio calculations

(1) The matrix elements of the molecular Hamiltonian are found from the electronic structure calculations performed along the minimum energy path (MEP) for the N–H bond elongation coordinate. The MEP is evaluated on a grid in the Jacobi coordinate R in the lowest excited state $^1A_2(\pi\sigma^*)$. The resulting energy profiles are shown in Fig. 1 of the main paper. Along the MEP, the molecule is constrained to C_{2v} geometries (i.e., $\theta, \phi = 0$). The aug-cc-pVTZ (AVTZ) basis set of Dunning[3] is used and further supplemented with the diffuse s and p functions added to the N and H atoms of the dissociating bond (one set of s and p functions for N and two sets for H). The exponents of these functions are derived in an even temprered manner from the most diffuse s and p functions of the AVTZ basis by dividing the exponents successively by a factor of 3.0.[4] This extension is necessary to correctly describe the Rydberg character of the A_2 and B_1 states.

(2) Most calculations are performed at the CASPT2 level of theory. The reference wavefunctions are obtained by state-averaged CASSCF calculations including the $\tilde{X}$, $^1A_2$ and $^1B_1$ states. The active space (eight electrons in seven orbitals) comprises five π valence molecular orbitals, three of b_1 and two of a_2 symmety, the $9a_1(\sigma)$ and the $10a_1(3s/\sigma^*)$ orbitals.

(3) Table I summarizes the characteristic features of the three calculated electronic states of pyrrole. Most researchers currently agree that the long wavelength absorption ($\lambda > 235\,\mathrm{nm}$) is due to the two lowest excited $^1\pi\sigma^*$ states with the vertical excitation energies T_v lying in the range $5.0 - 5.2\,\mathrm{eV}$ for the $^1A_2$ state and around $5.8 - 5.9\,\mathrm{eV}$ for the $^1B_1$ state.[5–9] This ordering of the electronic states at the Franck-Condon point is found in our CASPT2 calculations, too. Vertical excitation energies of the $\pi\sigma^*$ states are underestimated by 0.4 eV-0.6 eV compared to the CCSD and MRCI results; the calculated band origins T_0 agree with the known experimental values within similar bounds. The accuracy of the calculated dissociation thresholds is slightly better. Tables II and III provide further characterization of the molecular Hamiltonian and give the dimensionless coupling strength parameters $\kappa_c = \lambda/\omega$ for the coupling modes of a_2 and b_1 symmetries, respectively. The frequency ω is the pyrrolyl frequency at the respective intersection.

(4) The potential energies of the states $\tilde{X}$, A_2, and B_1 as functions of the disappearing modes are found on a three-dimensional grid in the (R_i, θ_j, ϕ_k)-space, with the nodes R_i being grid points on the MEP. The parameters of the $\mathbf{Q}$-dependent part of the Hamiltonian

TABLE I: Characteristic data of the ab initio potential energy surfaces of the three lowest electronic states of pyrrole: Vertical excitation energy T_v (in eV); band origin T_0 (in eV), which includes ZPEs of the ground and the excited electronic states; quantum mechanical thresholds D_0 for the electronic channels diabatically correlating with the calculated states (in eV). Available theoretical and experimental results are shown for comparison.

Diabatic state	T_v	T_0	T_0 (exp)	Dissociation channel	D_0[a]	D_0 (exp.)
$\tilde{X}^1A_1(\pi\pi)$	0.0	0.0	0.0	H(^1S)/pyrrolyl(1^2A_1)	5.09	–
	4.80[a]	4.32	<4.88[d]	H(^1S)/pyrrolyl(1^2A_2)	3.40	4.07[d]
$1^1A_2(\pi\sigma^*)$	5.17[b]					
	5.59[c]					
	5.45[a]	5.30	5.86[e]	H(^1S)/pyrrolyl(1^2B_1)	3.96	4.62 – 4.67[f]
$2^1B_1(\pi\sigma^*)$	5.88[b]					
	5.84[c]					

[a]This work; CASPT2.
[b]Ref. 8; CCSD.
[c]Ref. 9; MRCI.
[d]Ref. 10.
[e]Ref. 11.
[f]DFT[12] and MRCI[13] methods estimate the difference in the threshold energies $D_0(1^2B_1) - D_0(1^2A_2)$ to be in the range of 0.55 eV—0.60 eV.

TABLE II: Vibrational frequencies $\omega(i)$ (in cm^{-1}), coupling strengths λ_i (in cm^{-1}), and the dimensionless coupling strength parameters $\kappa_c = \lambda_c/\omega_c$ for the vibrational modes of a_2 symmetry at the X/A_2 conical intersection.

Mode	λ_c	ω_c	κ_c
$Q_{a2}(1)$	574.0	551.8	1.04
$Q_{a2}(2)$	759.0	895.7	0.85
$Q_{a2}(3)$	213.0	940.3	0.23

TABLE III: Vibrational frequencies $\omega(i)$ (in cm^{-1}), coupling strengths λ_i (in cm^{-1}), and the dimensionless coupling strength parameters $\kappa_c = \lambda_c/\omega_c$ for the vibrational modes of b_1 symmetry at the X/B_1 conical intersection. For the angle θ, λ_θ is evaluated as a gradient $\partial V/\partial(\sin\theta)$ at the intersection.

Mode	λ_c	ω_c	κ_c
θ	19751.00	854.00	23.12
$Q_{b1}(1)$	1151.00	823.6	1.40
$Q_{b1}(2)$	600.00	765.2	0.78
$Q_{b1}(3)$	265.00	875.3	0.30

are calculated as first and second derivatives with respect to deviations from the MEP. The complete ab initio protocol and the details of the diabatization procedure are described elsewhere.

(5) Coordinate dependent transition dipole moment (TDM) functions, necessary to properly describe the optical excitation of the $\pi\sigma^*$ states from the ground electronic state, are calculated at the CASSCF level of theory. Herzberg-Teller expansion is used to account for the dependence of the TDMs on the internal coordniates,

$$\boldsymbol{\mu}(\mathbf{R},\mathbf{Q}) \approx \boldsymbol{\mu}_R(\mathbf{R}) + \boldsymbol{\mu}_Q(\mathbf{Q})\,, \tag{7}$$

only linear deviations from the Franck-Condon geometry are taken into account. The coefficients in this expansion are calculated as numerical first derivatives of the TDMs with respect to nuclear displacements along the normal modes.

II. QUANTUM MECHANICAL CALCULATIONS

(1) The absorption spectra and the product state distributions, discussed in the main paper, are calculated using the Hamiltonian of Eq. (1) in which some coordinates are included in the dynamics while others are kept fixed to their asymptotic values. These coordinate choices are listed in Table IV. The results of the calculations using settings M1 and M3 are shown in Fig. 1 of the main paper; the results of the calculations M2 and M4 are shown in Figs. 2 and 3, respectively. Note that the vertical excitation energies depend on the number of included a_1 modes; the corresponding values are shown in Table IV. The dynamics of the

TABLE IV: Summary of the calculations reported in the main paper.

	Included states	Included coordinates	T_v [eV]	Transition dipole moment
M1.	X and A_2	$(R, Q_{a2}(3))$	3.96	$\mu = g_3 Q_{a2}(3)$
M2.	X and A_2	$(R, \theta, \phi, Q_{a1}(5), Q_{a2}(1), Q_{a2}(3))$	4.20	$\mu = g_1 Q_{a2}(1) + g_3 Q_{a2}(3)$
M3.	X and B_1	(R, θ)	5.69	$\mu = g_\theta \sin\theta$
M4.	X and B_1	(R, θ, ϕ)	5.69	$\mu = g_\theta \sin\theta \cos\phi$

coupled pairs of states X/A_2 and X/B_1 are studied separately, as was previously done in Ref. 4.

(2) Most of the reported calculations of the absorption spectra, bound and resonance eigenstates, and the product state distributions are performed using the program package PolyWave.[15] The code is applicable to general complex symmetric molecular Hamiltonians **H** represented as $N \times N$ matrices in the basis of N coupled diabatic electronic states. The time correlation functions, the energy dependent T-matrix elements, and the cross sections are calculated on equal footing using global in energy Chebyshev expansion of the propagator, thus allowing comparisons with both pump-probe and frequency resolved experiments. Filter diagonalization is performed in order to calculate the positions and widths of metastable resonance states reported in the main text and providing dynamical assignments of diffuse structures in the absorption spectra. The discrete variable representation (DVR) is used in the calculations. For the R coordinate, 100 potential optimized DVR points are used in the range $3.0\,a_0 - 14.0\,a_0$. For the angular coordinate θ, 100 Gauss-Legendre DVR points are used in the range $(0, \pi)$, and the coordinate ϕ is represented using 32 DVR points selected uniformly between 0 and 2π. The grids for the vibrational coordinates from the **Q**-space consist of up 32 potential optimized DVR points. The product state distributions are calculated using the method of Balint-Kurti et al.[16]

(3) The calculation M2 in Table IV is performed using the multi-configurational time-dependent Hartree method (MCTDH) as implemented in the Heidelberg MCTDH package.[17] The primitive grid in R consists of 98 sine DVR grid points chosen between 3.3 a_0 and 13.0 a_0; the (θ, ϕ)-dependent functions were represented using a two-dimensional Legendre DVR with $j_{\max} = 71$ and $m_{\max} = 21$; for the mode $Q_{a1}(5)$ 25 harmonic oscillator DVR grid points were used; for the modes $Q_{a2}(1)$ and $Q_{a2}(3)$ 17 harmonic oscillator

DVR points were used. The MCTDH wave function is expressed in the multi-set form expressed using five (combined) modes $\{R, (\theta, \phi), Q_{a1}(5), Q_{a2}(1), Q_{a2}(3)\}$ with the scheme of $\{(18, 16), (24, 11), (14, 10), (7, 6), (7, 6)\}$ single-particle functions for each combined mode and each state. Final state populations were calculated using the flux analysis method, as implemented in the MCTDH code.[18]

(4) The vibrational distributions of pyrrolyl in the in-plane mode $Q_{a1}(5)$ and in the coupling mode $Q_{a2}(1)$, obtained in the calculation M2 for the photon energy $E_{\rm ph} = 3.86\,$eV, corresponding to a Fano resonance, are compared in Fig. S3(a) and (b) with the distributions emerging in a direct dissociation (isolated state $^1A_2$). The distributions in the direct process (orange sticks) mainly reflect the projection of the initial state $\mu|\tilde{X}(\mathbf{0})\rangle$ onto the vibrations of the free pyrrolyl. Both the in-plane mode $Q_{a1}(5)$ and the coupling mode $Q_{a2}(1)$ remain cold (only $v = 0, 1$ are populated). Near resonance, these distributions spread to higher vibrational quantum numbers (blue sticks). This additional vibrational excitation is due to the dark diabatic component $|\tilde{X}(\mathbf{v})\rangle$ amplified by the coordinate dependence of the vibronic coupling $\hat{H}_{\rm CI}$. The vibronic coupling is weak, and the extra excitation due to $\hat{H}_{\rm CI}|\tilde{X}(\mathbf{v})\rangle$ is limited to few quanta. Since the vibronic coupling is linear in the a_2 modes, the sequence of two diabatic transfers [Eqs. (2) and (3) of the main text] can induce an excitation by maximum two quanta in the coupling modes.

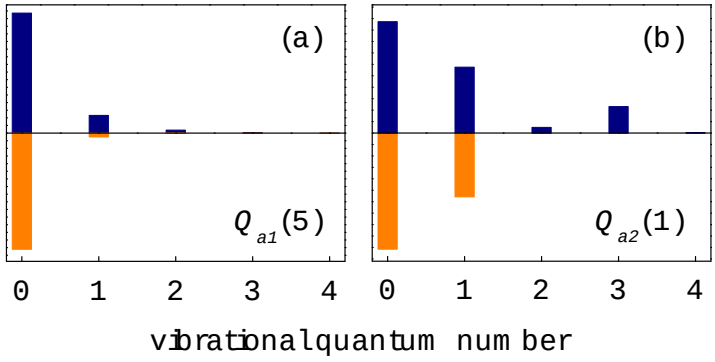

FIG. S3: (a) The vibrational distribution for the pyrrolyl mode $Q_{a1}(5)$ calculated for the excitation energy $E_{\rm ph} = 3.86\,$eV, corresponding to a Fano resonance, as a blue stick. The distribution calculated at the same energy for the isolated state $^1A_2(\pi\sigma^*)$ is shown with orange color. (b) The same as in (a), but for the pyrrolyl mode $Q_{a2}(1)$.

Note that the experimental detection of the interference structures in the photofragment distributions can be hindered by the small width of Fano resonances. For example, the

photofragment kinetic energy measurements of Ashfold and co-workers,[10] performed at fixed photolysis wavelengths, can easily miss narrow resonance states. In contrast, PHOFEX spectra of pyrrole, discussed in the main text, are well suited to resolve the interference effects emerging from the conical intersection.

[1] H. Köppel, L. S. Cederbaum, and W. Domcke, Adv. Chem. Phys. **57**, 59 (1984)

[2] H. Köppel, J. Gronki, and W. Domcke, J. Chem. Phys. **115**, 2377 (2001)

[3] T. H. Dunning, J. Chem. Phys. **90**, 1007 (1989)

[4] V. Vallet, Z. Lan, S. Mahapatra, A. L. Sobolewski and W. Domcke, J. Chem. Phys. **123**, 144307 (2005)

[5] B. O. Roos, P. A. Malmqvist, V. Molina, L. Serrano-Andrés and M. Merchán, J. Chem. Phys **116**, 7526 (2002)

[6] X. Li and J. Paldus, J. Phys. Chem. A **114**, 8591 (2010)

[7] S. P. Neville and G. A. Worth, J. Chem. Phys. **140**, 034317 (2014)

[8] O. Christiansen, J. Gauss, J. F. Stanton, and P. Jorgensen, J. Chem. Phys. **111**, 525 (1999)

[9] M. H. Palmer and P. J. Wilson, Mol. Phys. **101**, 2391 (2003)

[10] B. Cronin, M. G. D. Nix, R. H. Qadiri and M. N. R. Ashfold, PCCP **6**, 5031 (2004)

[11] M. H. Palmer, I. C. Walker and M. F. Guest, Chem. Phys. **238**, 179 (1998)

[12] A. J. Gianola, T. Ichino, R. L. Hoenigman, S. Kato, V. M. Bierbaum and W. C. Lineberger, J. Phys. Chem. A **108**, 10326 (2004)

[13] A. Motzke, Z. Lan, C. Woywod and W. Domcke, Chem. Phys. **329**, 50 (2006)

[14] W. H. Miller, N. C. Handy, and J. E. Adams, J. Chem. Phys. **72**, 99 (1979)

[15] 'PolyWave' is a package of FORTRAN90 programs for iterative quantum mechanical calculations of bound states, dissociative resonance states, photoabsorption or photoemission spectra, as well as product state distributions in molecules with up to six internal degrees of freedom and $N \leq 9$ coupled electronic states. The package is available from the author upon request.

[16] G. G. Balint-Kurti, R. N. Dixon, and C. C. Marston, J. Chem. Soc. Faraday Trans. **86**, 1741 (1990)

[17] G. A. Worth, M. H. Beck, A. Jäckle, and H.-D. Meyer. The MCTDH Package, version 8.4, see http://mctdh.uni-hd.de

[18] A. Jäckle and H.-D. Meyer, J. Chem. Phys. **105**, 6778 (1996)